Regulation of Inducible Nitric Oxide Synthase by Self-Generated NO†

Husam M. Abu-Soud,*,‡ Kohji Ichimori,§ Hiroe Nakazawa,§ and Dennis J. Stuehr*,‡

Departments of Immunology and Cell Biology, Lerner Research Institute, The Cleveland Clinic, Cleveland, Ohio, 44195 and the Department of Physiology, Tokai University, Bohseidai, Isehara, Japan 259-1193

Received January 10, 2001

ABSTRACT: A ferric heme−nitric oxide (NO) complex can build up in mouse inducible nitric oxide synthase (iNOS) during NO synthesis from L-arginine. We investigated its formation kinetics, effect on catalytic activity, dependence on solution NO concentration, and effect on enzyme oxygen response (apparent KmO_2). Heme−NO complex formation was biphasic and was linked kinetically to an inhibition of electron flux and catalysis in iNOS. Experiments that utilized a superoxide generating system to scavenge NO showed that the magnitude of heme−NO complex formation directly depended on the NO concentration achieved in the reaction solution. However, a minor portion of heme−NO complex (20%) still formed during NO synthesis even when solution NO was completely scavenged. Formation of the intrinsic heme−NO complex, and the heme−NO complex related to buildup of solution NO, increased the apparent KmO_2 of iNOS by 10- and 4-fold, respectively. Together, the data show heme−NO complex buildup in iNOS is due to both intrinsic NO binding and to equilibrium binding of solution NO, with the latter predominating when NO reaches high nanomolar to low micromolar concentrations. This behavior distinguishes iNOS from the other NOS isoforms and indicates a more complex regulation is possible for its activity and oxygen response in biologic settings.

In animals, nitric oxide (NO)[1] is generated from L-arginine (Arg) by three main isoforms of NO synthase (NOS): neuronal (nNOS or NOS I), macrophage (iNOS or NOS II), and endothelial (eNOS or NOS III). The NOS isoforms differ in their primary sequences, mode of expression, cellular location, and biologic function (see refs *1*−*4* for review) but all catalyze an identical two-step reaction to generate NO. The NOS are composed of an N-terminal oxygenase domain that contains heme, 6R-tetrahydrobiopterin (H_4B), and the Arg binding site, a central calmodulin binding sequence, and a C-terminal reductase domain that contains FAD, FMN, and an NADPH binding site (*5*). The reductase domain transfers NADPH-derived electrons to the oxygenase domain for O_2 activation and NO synthesis, and the NOS heme is responsible for binding and activating O_2 (*6*, *7*). The heme iron is ligated to the protein through a cysteine thiolate and can bind a variety of alternative molecules as sixth ligands, including CO, NO, CN, and imidazoles (*8*−*12*). Crystal structures of NOS oxygenase domains reveal an unusual topology and heme environment that are in several ways distinct from cytochrome P-450s or other heme proteins (*13*−*15*).

Because NOSs are heme proteins they are susceptible to product inhibition by NO. This was first demonstrated by adding NO donors during enzyme assay (*16*, *17*). We and others have characterized a reversible inhibition that is related to the NOS heme binding self-generated NO (*9*, *18*−*26*). Heme−NO complex buildup severely inhibits steady-state catalysis by nNOS (*18*, *24*, *25*). In addition, it greatly increases the enzyme's apparent KmO_2 (*19*, *24*) and thus may regulate its activity in physiologic settings. Interesting differences have emerged among the NOS isoforms regarding the extent and type of heme−NO complex that accumulate. For example, approximately 70% of nNOS molecules partition during NO synthesis into a ferrous heme−NO complex, and both its complex buildup and catalytic inhibition are insensitive to the solution NO concentration (*18*, *23*). In eNOS, much less heme−NO complex buildup occurs (*20*), consistent with its relatively slow catalytic rate. A majority of iNOS can also partition into a heme−NO complex during catalysis (*9*). However, its heme−NO complex is predominantly ferric, and the catalytic inhibition associated with its formation can be largely eliminated by an added NO scavenger such as oxyhemoglobin. These different behaviors among the NOS isoforms are not related to different NO binding affinities, which are fairly similar (*20*, *27*−*30*).

To better understand how self-generated NO regulates iNOS, we closely compared how the kinetics of its heme−NO complex formation is associated with catalytic inhibition. We also investigated if varying the NO concentration achieved in solution would alter the extent of its heme−NO complex formation, and if this in turn would alter catalytic inhibition and shift in enzyme apparent KmO_2. Our results show that heme−NO complex formation in iNOS is pre-

† This work was supported by National Institutes of Health Grants GM51491 and CA53914 to D.J.S., a grant from the American Heart Association to H.A.S., and Grant-in-Aid for International Scientific Research No. 10045076 to H.N.

* To whom correspondence should be addressed: Department of Immunology NB-3 (for D.J.S.), and Department of Cell Biology NN-1 (for H.A.S.), Lerner Research Institute, Cleveland Clinic, 9500 Euclid Ave., Cleveland, OH 44195. Fax: 216-444-9329 (D.J.S.); 216-444-9404 (H.A.S.); e-mail: stuehrd@ccf.org and abusouh@ccf.org.

‡ Lerner Research Institute.

§ Tokai University.

[1] Abbreviations: Arg, L-arginine; eNOS, bovine endothelial NOS; H4B, (6 *R*)-5,6,7,8-tetrahydro-L-biopterin; iNOS, mouse inducible NOS; nNOS, rat neuronal NOS; NO, nitric oxide; NOS, NO synthase; SOD, superoxide dismutase.

10.1021/bi010066m CCC: $20.00
Published on Web 05/15/2001

dominantly regulated through equilibrium binding of solution NO to its ferric heme. This distinguishes iNOS from nNOS and allows for a more complex regulation of its biologic activity.

MATERIALS AND METHODS

Materials. Hypoxanthine, manganese superoxide dismutase (SOD), and cytochrome *c* were obtained from Sigma. Xanthine oxidase from cow milk was purchased from Boehringer Mannheim, Indianapolis. Other chemicals and reagents were obtained from Sigma or from sources previously reported (*18*, *20*, *27*). Full-length mouse iNOS was expressed in *Escherichia coli* and purified to homogeneity in the presence of H4B as previously described (*31*).

Optical Spectroscopy During iNOS NO Synthesis. Spectra of iNOS prior to, during, and following catalysis were recorded in cuvettes at 15 °C in a final volume of 1 mL using a Hitachi U3010 spectrophotometer equipped with a thermostated cuvette holder. Reactions were monitored either by wavelength scanning or by monitoring the change in absorbance at 436 and 340 nm over time (*18*). For a typical reaction, iNOS was diluted to 1 μM in air-saturated 40 mM Bis-tris propane buffer, pH 7.4, containing 4 μM H4B, 0.2 mM DTT, and 1 mM Arg. NADPH was added to initiate NO synthesis as noted in the text. For experiments that required measurement of citrulline or Arg by HPLC, 40 mM Hepes was used in place of BIS-Tris propane buffer. The enzyme concentration was determined spectrophotometrically based on an estimated extinction coefficient of 76 mM^{-1} cm^{-1} per heme.

Measurement of iNOS NO Synthesis and NADPH Oxidation at Different O_2 Concentrations. Experiments were performed using conditions as previously detailed (*19*, *20*). Concentrated iNOS (8.7 μg) was placed in septum-sealed cuvettes and diluted with various ratios of N_2-, air-, or O_2-saturated buffer solutions that contained 40 mM Bis-tris propane, pH 7.4, 1 mM Arg, 0.5 mM DTT, and 4 μM each of FMN, FAD, and H4B (final volume 1 mL). In some cases, the cuvette also contained 10 μM oxyhemoglobin. The initial O_2 concentration in each reaction was calculated based on the solution mixing ratio and the O_2 concentration of air or O_2-saturated buffer at 25 °C (approximately 0.26 and 1.26 mM, respectively). Reactions were initiated by injecting 10 μL NADPH (0.1 mM final concentration) and run at 25 °C. The rate of NADPH oxidation was determined at 340 nm in the presence or absence of Arg and in the presence or absence of oxyhemoglobin. Apparent KmO_2 values were estimated from double reciprocal plots of the rate data as described in the text.

Rapid Kinetic Measurements. Heme−NO complex formation was followed at 436 nm using a stopped-flow instrument from Hi-Tech Ltd. (model SF-51). This wavelength can detect both ferric and ferrous heme−NO complexes of iNOS. Experiments were performed at 15 °C. A solution containing 2 μM iNOS in 40 mM bis-tris propane, pH 7.4, 0.5 mM DTT, 4 μM H4B, and 1 mM Arg was rapidly mixed with an air-saturated buffer solution that contained 140 μM NADPH. NADPH consumption was monitored in replica reactions at 340 nm. In all cases, 5−10 successive scans were combined to generate an average and analyzed using of a nonlinear least-squares method provided by the instrument manufacturer.

Electrochemical Detection of NO. NO was measured using an NO meter (ISO-NO Mark II) connected with an ISO-NOP 200 sensor (World Precision Instruments, Inc., Sarasota, USA). The applied voltage was +865 mV, and the low pass filter for noise reduction was set to 1 Hz. The electrode current was recorded with a DT recorder (model 1202, Linear Instruments Corp, USA). The NO measurements were performed in a 4-mL cell that was surrounded by a thermostated water jacket to maintain constant temperature. The reactions were stirred, and the temperature was kept at 15 °C in all experiments. Calibration of the electrode was performed by the stepwise addition of a NO solution (1 μL each) to 3 mL of argon-deoxygenated buffer (40 mM HEPES, pH 7.4, 15 °C) in a stirred, rubber-sealed cell. The concentration of the standard NO solution was determined by rapidly mixing 1−5 μL with 1 mL of oxyhemoglobin solution (8 μM in 40 mM HEPES, pH 7.4) and monitoring the absorbance increase at 401 nm (extinction difference coefficient = 38 mM^{-1} cm^{-1}). The electrode current was proportional to NO concentration up to 10 μM, and sensitivity of the electrode was typically 410 nM NO/nA.

Detection of NO from iNOS. iNOS (0.5 μM) was incubated at 15 °C for 5 min in 40 mM HEPES buffer, pH 7.4, containing 0.2 mM Arg, 0.3 mM DTT, and 4 μM H4B. NADPH (70 μM) was added to start the enzyme reaction, and the total reaction volume was 2 mL. The electrode current was monitored on a chart recorder with continuous stirring of the reaction solution.

Assay of Citrulline Formation. After initiating NO synthesis, 10 μL aliquots were removed from reactions at timed intervals, and the enzyme activity was immediately quenched by mixing with 1 μL of 5 N HCl. Citrulline in the samples was derivatized with *o*-phthalaldehyde and quantitated using a fluorometric HPLC method with standard citrulline samples as reference (*20*).

Effect of a Superoxide-Generating System on NO Buildup, iNOS Activity, and Heme−NO Complex Formation. Identical reactions were run in an unstirred cuvette or in the stirred open vessel used for NO electrode measurements. iNOS (0.5 μM) was incubated at 15 °C for 5 min in the reaction solution described above plus 1.2 mM of hypoxanthine. Thirty seconds after xanthine oxidase was added to the solution, 70 μM NADPH was added to start NO synthesis. NADPH consumption and heme−NO complex formation in the cuvette reaction were monitored at 340 nm and at 436 nm, respectively, and the NO concentration in the open vessel was monitored with the electrode. The rate of superoxide production in the reactions was estimated by measuring the rate of SOD-inhibitable cytochrome *c* reduction as follows: HEPES buffer (40 mM, pH 7.4) containing 1.2 mM hypoxanthine, catalase (1300 U/mL), and 50 μM cytochrome *c* was incubated at 15 °C. Different amounts of xanthine oxidase were added to start the reaction and the reduction of cytochrome *c* was monitored at 550 nm. Replica reactions that contained manganese SOD (100 U/mL) were run to calculate the SOD-inhibitable portion of cytochrome *c* reduction. Below 0.3 U/mL of xanthine oxidase, the rate of SOD-inhibitable superoxide production displayed a linear relationship to xanthine oxidase concentration.

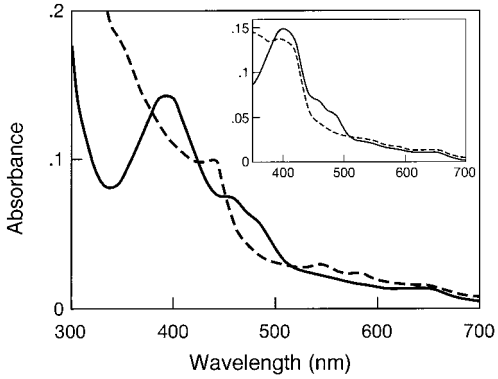

FIGURE 1: Light absorbance spectra of iNOS prior to and during catalysis. The main panel shows ferric iNOS before (solid line) and after initiating NO synthesis from Arg (dashed line). The inset shows iNOS before (solid line) and after adding NADPH (dashed line) in the absence of Arg.

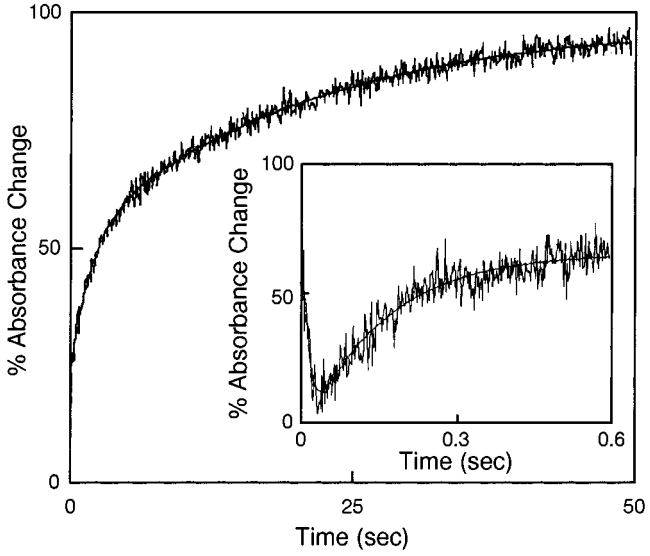

FIGURE 2: Kinetics of heme−NO complex formation in iNOS. NO synthesis was initiated by rapid mixing a solution containing iNOS, Arg, and H4B with a solution containing NADPH at 15 °C. Heme−NO complex formation was followed at 436 nm in a stopped-flow spectrophotometer. The inset shows absorbance change from the same trace within an initial time period. Traces contain lines of best fit that were calculated using a two-exponential equation to describe absorbance change.

RESULTS

Formation of a Ferric Heme−NO Complex during Steady-State Catalysis. Addition of NADPH to initiate NO synthesis from Arg converted iNOS to a species displaying Soret absorbance at 440 nm and two well-resolved visible peaks at 542 and 578 nm (Figure 1). These spectral features match those of authentic ferric-NO iNOS (*9*, *10*) and confirm that a majority of iNOS exists as a ferric heme−NO complex during steady-state catalysis under these conditions (*9*). The heme−NO complex did not form when iNOS was allowed to oxidize NADPH in the absence of Arg (Figure 1 inset). Instead, the steady state spectrum showed that the enzyme flavins were in a reduced state and the heme was predominantly in ferric form.

Kinetics of Heme−NO Complex Formation. We utilized stopped-flow spectroscopy to examine buildup of the iNOS heme−NO complex during the initial phase of NO synthesis. The reaction was initiated at 15 °C by mixing an anaerobic solution of iNOS, H4B, and Arg with an air-saturated solution of NADPH. Heme−NO complex formation was followed at 436 nm, a wavelength that detects both ferrous and ferric heme−NO complexes of NOS. We observed an initial rapid decrease in absorbance in the first 10 ms that is attributed to flavin reduction by NADPH (*18*, *26*) (Figure 2 inset). This was followed by an increase in absorbance over the next 50 s that can be attributed to heme−NO complex formation (Figure 2 main panel). Flavin reduction was best fit to a single-exponential function, giving $k_{obs} = 90\ s^{-1}$. In contrast, heme−NO complex buildup was best described as a biphasic process (observed rate constants $k_1 = 6.5\ s^{-1}$ and $k_2 = 0.05\ s^{-1}$) with the slower phase representing a majority (approximately 70%) of the absorbance increase at 436 nm.

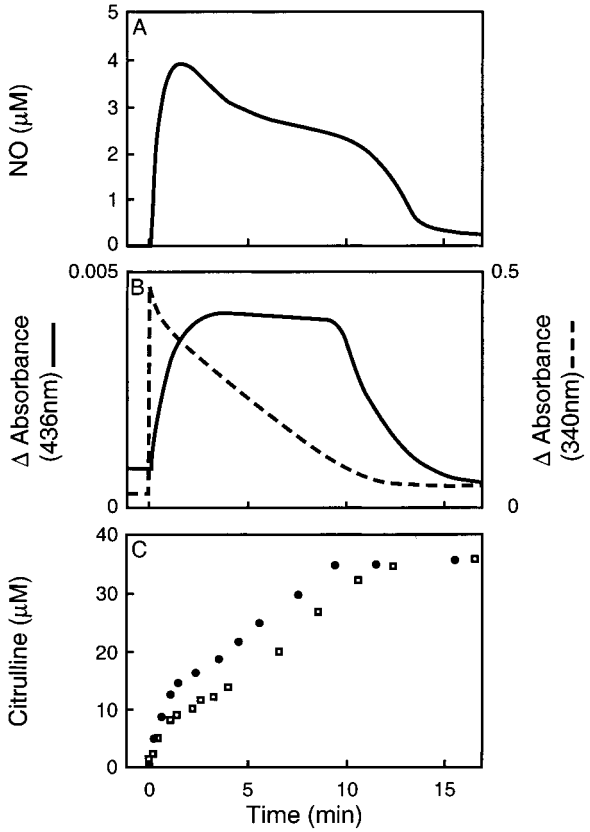

FIGURE 3: Relationship between NO buildup in solution, heme−NO complex formation, rate of NADPH consumption, and rate of product formation in iNOS. Reactions were initiated by adding NADPH at time zero to a solution of enzyme containing Arg and H4B at 15 °C. Panel A illustrates NO concentration versus time in the reaction. Panel B shows the kinetics of heme−NO complex formation in iNOS as determined at 436 nm, and NADPH consumption as determined at 340 nm. Panel C shows the kinetics of citrulline accumulation in the reaction of panels A (open squares) and B (solid circles). The data are representative of at least three experiments each.

Relationship between NO Concentration, Heme−NO Complex Formation, and Catalytic Activity. Figure 3 shows how the NO concentration in the reaction changes after initiating NO synthesis by iNOS and compares this to changes in heme−NO complex formation and rates of NADPH oxidation or citrulline formation. As shown in panel A, the NO concentration increased over the first minute, reached a peak, decreased slowly for around 7 min, and then decreased more rapidly over 3 min. Panel B shows that the increase in NO concentration correlated with buildup of the iNOS heme−NO complex and a deflection in the rate of NADPH

oxidation. The intermediate period where near constant NO concentration was observed was associated with a steady amount of heme−NO complex present and a steady rate of NADPH oxidation by iNOS. The final period of faster NO loss took place as all the NADPH became consumed and correlated with decay of the iNOS heme−NO complex. Panel C shows that NO buildup in solution and heme−NO complex formation were associated with an equivalent deflection in the initial rate of citrulline formation for both the NO electrode reaction and the cuvette reaction. This deflection was followed by a slower steady-state rate until all NADPH was consumed. We conclude: (i) Heme−NO complex buildup lowers global iNOS activity. (ii) The kinetics of heme−NO complex buildup, duration, and decay largely match NO accumulation in the iNOS reaction mixture.

Effect of a NO Scavenging System. To test these conclusions, we examined how graded superoxide production would affect NO accumulation, heme−NO complex formation, and catalysis by iNOS. Because superoxide reacts with NO at a near diffusion-controlled rate (6.7×10^9 M^{-1} s^{-1}), its production should lower the NO concentration achieved during the iNOS reaction, which should in turn decrease heme−NO complex formation and increase rates of steady-state catalysis. As shown in the upper panel of Figure 4, adding graded amounts of a xanthine oxidase superoxide-generating system lowered the NO levels achieved in the iNOS reaction and also decreased the duration of the reaction. NO did not accumulate to detectable levels in the reaction that received the highest amount of xanthine oxidase. The changes in NO concentration correlated with less heme−NO complex formation by iNOS and a shorter duration for the heme−NO complex (Figure 4, middle panel). However, a minor amount (approximately 20%) heme−NO complex still accumulated even when solution NO was undetectable. This held true even when superoxide generation in the system was additionally increased by a factor of 3 (data not shown). Wavelength scans recorded in the presence of the superoxide generating system (at 0.05 or 0.1 U/mL of xanthine oxidase) confirmed that the residual 436 nm absorbance represented an iNOS heme−NO complex (data not shown).

Lowering the NO concentration with the superoxide generating system also correlated with less deflection in the NADPH oxidation rate and a decreased duration for the reaction (Figure 4, lower panel). The highest rate of iNOS catalysis was associated with undetectable NO buildup, no discernible deflection in its rate of NADPH consumption and minimal heme−NO complex formation during the steady state. Together, these results show how solution NO can control heme−NO complex buildup and catalysis in iNOS.

Effect of NO in Modulating the Apparent KmO_2 of iNOS. To see if NO buildup alters iNOS activity versus O_2 response, we measured its catalytic activity versus O_2 concentration under three conditions: (i) NO synthesis with NO allowed to accumulate in solution, (ii) NO synthesis in the presence of oxyhemoglobin to scavenge NO, and (iii) catalysis without NO synthesis (no Arg). In all cases, steady state rates of NADPH oxidation were used as a common marker of catalytic activity. Panels A−C of Figure 5 contain reciprocal plots of the rate data obtained under the three different conditions. These gave apparent KmO_2 values of 130 μM when NO was allowed to accumulate during NO synthesis, 42 μM when NO is synthesized but is scavenged by added oxyhemoglobin, and 3 μM when no NO synthesis occurred. Thus, both NO synthesis and NO buildup in solution caused the apparent KmO_2 of iNOS to increase. For comparison, these iNOS apparent KmO_2 values are listed in Table 1 with values obtained for nNOS and eNOS under similar experimental conditions.

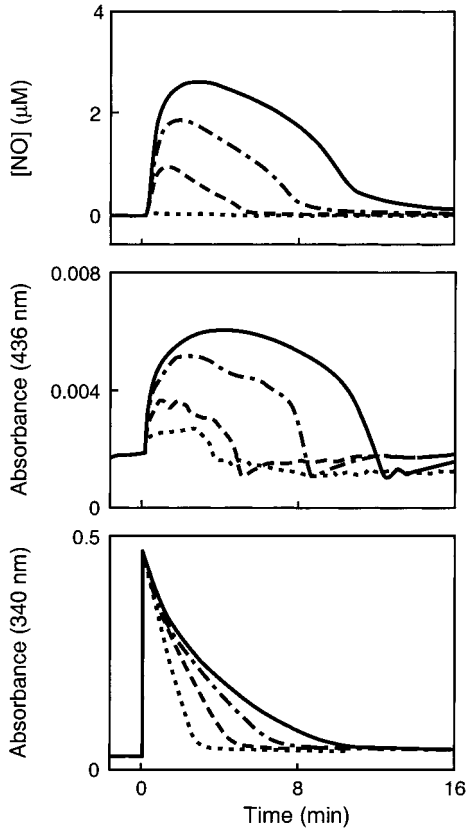

FIGURE 4: Relationship between NO concentration achieved during the reaction, heme−NO complex formation, and rate of catalysis by iNOS. Reactions were initiated by adding NADPH at time zero to a solution of enzyme containing Arg and H4B at 15 °C. Reactions also contained a superoxide generating system consisting of hypoxanthine plus 0 (solid), 0.02 (dash−dot), 0.05 (dash), or 0.1 (dot) U/mL xanthine oxidase. This generated 0, 2.7, 7.1, and 14.4 μM superoxide/min, respectively, in the reactions. See Materials and Methods for details. Top panel: NO concentration during each reaction. Middle panel: iNOS heme−NO complex formation as measured at 436 nm. Lower panel: NADPH consumption rate as measured at 340 nm. The data are representative of at least three experiments each.

DISCUSSION

Our results confirm that NO synthesis causes buildup of a six-coordinate ferric heme−NO complex in iNOS (*9*). Moreover, they show that heme−NO complex formation is kinetically linked to an inhibition of NADPH consumption and citrulline production by iNOS and causes a shift in iNOS apparent KmO_2 to higher values. Together, this makes iNOS operate at a fraction of its maximum activity in the steady state and significantly alters its activity response within the physiologic concentration range of O_2 (0−200 μM).

Although heme−NO complex formation inhibits iNOS and nNOS catalysis in a similar way, there are important differences in the fundamental aspects. For example, heme−NO complex buildup is biphasic in both iNOS and nNOS (*18*), but for iNOS the second phase is much slower. In

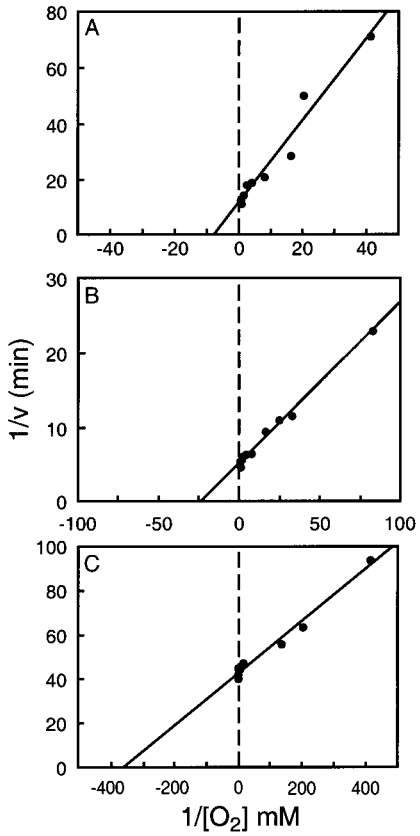

FIGURE 5: Double reciprocal plots of iNOS activity versus O_2 concentration under three reaction conditions. Catalysis was initiated at 25 °C by adding NADPH to cuvettes containing iNOS and various concentrations of O2 in a cuvette. Activity was measured as the rate of NADPH oxidation at 340 nm over the first 4 min of the reaction. Reactions contained Arg without a NO scavenger (A), Arg and oxyhemoglobin (B), or no Arg (C).

Table 1: Effect of NO Synthesis and Solution NO on Apparent KmO_2 for Three NOS Isoforms

assay condition	apparent KmO_2 (μM)		
	iNOS	eNOS[a]	nNOS[a]
+ substrate[b]	130	4 (25)	350
+ substrate, + oxyhemoglobin	42	ND[c]	340
− Arg	3	ND	38

[a] Values for eNOS and nNOS taken from refs *20* and *19*, respectively. [b] Values obtained using Arg as substrate or using *N*-hydroxy-L-arginine (value noted in parentheses). [c] ND, not determined.

addition, its magnitude can be greatly reduced by an added NO scavenger. This is consistent with heme−NO complex buildup being due to two distinct binding events: NO binding to the heme before it leaves the active site (*32*) and the heme binding NO that accumulates in solution.

The existence of a first phase, "preequilibrium" NO binding event is indicated by our observing that about 20% heme−NO complex remained during steady-state catalysis even when the solution NO concentration was reduced to an undetectable level. It is also consistent with single turnover or flash photolysis studies done with eNOS (*29*), nNOS (*30*, *32*), and iNOS[2] that indicate practically all newly formed NO binds to the ferric NOS heme before leaving the active site. Thus, during our steady state measurement it appears that a minor proportion of iNOS enzyme molecules still contained bound NO from this initial binding event. The magnitude of this subpopulation is presumably influenced by the relative rates of NO formation versus NO dissociation from the ferric heme (*24*) and for iNOS represents a minority of the total enzyme during the steady state.

As noted above, the second phase of NO complex formation was slow in iNOS and its magnitude depended on the NO concentration achieved in the reaction solution. The slow phase of buildup was not limited by the rates of heme reduction or NO dissociation from the heme, which are about 40 times faster (*20*) and thus is not linked to the rate of NO synthesis. Instead, it likely reflects a binding equilibrium between the ferric heme and NO that builds up in solution. In the cuvette reactions, NO concentrations were apparently sufficient to allow a significant percentage of iNOS heme to bind solution NO. The degree of NO complex formation that was observed is consistent with the estimated affinity of NO toward the iNOS ferric heme as determined in stopped flow, flash photolysis, and scavenging experiments (*27*, *30*, *32*) and with the measured NO concentrations in the reactions. Together these predict that high nanomolar to low micromolar concentrations of NO are required for significant equilibrium binding.

Binding solution NO can also explain why the heme−NO complex that builds up during iNOS catalysis is predominantly ferric. Consider that reduction of ferric heme is the slow step in NO synthesis for iNOS (*7*, *24*).[3] Thus, a majority of iNOS exists in ferric form during steady state catalysis in air-saturated buffer (see Figure 1) and so would be predominantly available to bind solution NO when appropriate concentrations are reached. This differs from nNOS, which after initiating NO synthesis quickly accumulates as a ferrous heme−NO complex independent of the solution NO concentration (*18*). In that case, complex buildup involves reduction of an initial ferric heme−NO complex that forms as an immediate product of catalysis (*32*) and does not involve equilibrium binding of solution NO to the heme. Although a ferric heme−NO complex also forms as an immediate product of iNOS catalysis,[2] we suspect it may be reduced more slowly as compared to nNOS or be less stable after it becomes reduced, such that a ferrous heme−NO complex does not accumulate during the steady state. This allows the ferric enzyme to predominate and bind NO once its concentration builds in solution.

Increases in apparent KmO_2 for iNOS, nNOS, and eNOS are all linked to heme−NO complex formation during catalysis (*19*, *20*, *24*). However, the basis for the effect must differ in iNOS as compared to nNOS. In iNOS, we actually discerned two shifts in the apparent KmO_2 (Table 1). One shift occurred during NO synthesis in the presence of a NO scavenger, while the second shift occurred when NO was allowed to accumulate in solution during catalysis. This is not the case for nNOS, whose shift in apparent KmO_2 is almost unaffected by buildup of solution NO and therefore much more invariant in the presence or absence of a NO scavenger (Table 1). Thus, when external NO is scavenged there is still an effect of NO synthesis on the apparent KmO_2

[2] Wang, Z.-Q., Wei, C.-C., and Stuehr, D. J., manuscript in preparation.

[3] Santolini, J., and Stuehr, D. J., manuscript in preparation.

of iNOS, but this isoform also remains susceptible to an effect related to the external NO concentration. The second effect can be substantial if NO concentrations build up to low micromolar levels during catalysis. We are continuing to explore the basis for this difference among NOS isoforms.

Biological Implications. iNOS binding self-generated NO inhibits its rate and increases its apparent KmO_2. This alone may be important in biologic settings where iNOS is expressed. That its heme−NO complex formation is largely dependent on solution NO adds another level of complexity because it means the cellular environment can control the extent of NO regulation in iNOS. Thus, any changes that alter cellular superoxide levels or exposure to NO scavengers such as oxyhemoglobin, O_2, or peroxidases (*33*−*35*) will potentially affect cellular NO levels and in turn change iNOS activity and O_2 response through an effect on heme−NO complex formation. Such changes in iNOS function should be reversible and dynamic and occur in concert with changes in environmental NO concentration. There already is evidence that significant iNOS heme−NO complex formation occurs in vivo to regulate its function: NO concentrations in normal human airway appear to be sufficiently high to shift the apparent KmO_2 of iNOS to approximately 190 μM (*36*), which is similar to the value observed for purified iNOS when generating micromolar concentrations of NO (see Table 1). Evidence suggests this effect on lung iNOS may be coupled to physiologic O_2 response in the lung (*36*). Thus, understanding how heme−NO binding regulates each NOS isoform may lead to a better understanding of their varied biologic functions.

ACKNOWLEDGMENT

We thank Dr. Jerome Santolini for reviewing the manuscript.

REFERENCES

1. Hobbs, A. J., Higgs, A., and Moncada, S. (1999) *Annu. Rev. Pharmacol. Toxicol. 39*, 191−220.
2. Hemmens, B., and Mayer, B. (1997) in *Methods in Molecular Biology* (Titheradge, M. A., Ed.) Vol. 100, pp 1−32, Humana Press, Totowa, NJ.
3. Nathan, C., and Shiloh, M. U. (2000) *Proc. Natl. Acad. Sci. U.S.A. 97*, 8841−8.
4. Zamora, R., Vodovotz, Y., and Billiar, T. R. (2000) *Mol. Med. 6*, 347−73.
5. Stuehr, D. J. (1999) *Biochim. Biophys. Acta 1411*, 2146−2152.
6. Gorren, A. C., Bec, N., Schrammel, A., Werner, E. R., Lange, R., and Mayer, B. (2000) *Biochemistry 39*, 11763−70.
7. Wei, C. C., Wang, Z. Q., Wang, Q., Meade, A. L., Hemann, C., Hille, R., and Stuehr, D. J. (2001) *J. Biol. Chem. 276*, 315−319.
8. Jung, C., Stuehr, D. J., and Ghosh, D. K. (2000) *Biochemistry 39*, 10163−71.
9. Hurshman, A. R., and Marletta, M. A. (1995) *Biochemistry 34*, 5627−5634.
10. Wang, J., Rousseau, D. L., Abu-Soud, H. M., and Stuehr, D. J. (1994) *Proc. Natl. Acad. Sci. U.S.A. 91*, 10512−10516.
11. Matsuoka, A., Stuehr, D. J., Olson, J. S., Clark, P., and Ikeda-Saito, M. (1994) *J. Biol. Chem. 269*, 20335−20339.
12. McMillan, K., Adler, M., Auld, D. S., Baldwin, J. J., Blasko, E., Browne, L. J., Chelsky, D., Davey, D., Dolle, R. E., Eagen, K. A., Erickson, S., Feldman, R. I., Glaser, C. B., Mallari, C., Morrissey, M. M., Ohlmeyer, M. H., Pan, G., Parkinson, J. F., Phillips, G. B., Polokoff, M. A., Sigal, N. H., Vergona, R., Whitlow, M., Young, T. A., and Devlin, J. J. (2000) *Proc. Natl. Acad. Sci. U.S.A. 97*, 1506−11.
13. Crane, B. R., Arvai, A. S., Gachhui, R., Wu, C., Ghosh, D. K., Getzoff, E. D. Stuehr, D. J., and Tainer, J. A. (1997) *Science 278*, 425−431.
14. Li, H., Raman, C. S., Glaser, C. B., Blasko, E., Young, T. A., Parkinson, J. F., Whitlow, M., and Poulos, T. L. (1999) *J. Biol. Chem. 274*, 21276−84.
15. Fischmann, T. O., Hruza, A., Niu., X. D., Fossetta, J. D., Lunn, C. A., Dolphin, E., Prongay, A. J., Reichert, P., Lundell, D. J., Narula, S. K., and Weber, P. C. (1999) *Nat. Struct. Biol. 6*, 233−242.
16. Rogers, N. E., and Ignarro, L. J. (1992) *Biochem. Biophys. Res. Commun. 189*, 242−245.
17. Rengasamy, A., and Johns, R. A. (1993) *Mol. Pharmacol. 44*, 124−8.
18. Abu-Soud, H. M., Wang, J., Rousseau, D. L., Fukuto, J. M., Ignarro, L. J., and Stuehr, D. J. (1995) *J. Biol. Chem. 270*, 22997−23006.
19. Abu-Soud, H. M., Rousseau, D. L., and Stuehr, D. J. (1996) *J. Biol. Chem. 271*, 32515−32518.
20. Abu-Soud, H. M., Ichimori, K., Presta, A., and Stuehr, D. J. (2000) *J. Biol. Chem. 275*, 17349−57.
21. Gorren, A. C., Schrammel, A., Riethmuller, C., Schmidt, K., Koesling, D., Werner, E. R., and Mayer, B. (2000) *Biochem. J. 347*, 475−484.
22. Miller, R. T., Martasek, P., Omura, T., and Masters, B. S. (1999) *Biochem. Biophys. Res. Commun. 265*, 184−188.
23. Nishimura, J. S., Narayanasami, R., Miller, R. T., Roman, L. J., Panda, S., and Masters, B. S. (1999) *J. Biol. Chem. 274*, 5399−5406.
24. Santolini, J., Adak, S., Curran, C. M. L., and Stuehr, D. J. (2001) *J. Biol. Chem. 276*, 1233−1243.
25. Adak, S., Wang, Q., and Stuehr, D. J. (2000) *J. Biol. Chem. 275*, 17434−17439.
26. Roman, L. J., Martasek, P., Miller, R. T., Harris, D. E., de La Garza, M. A., Shea, T. M., Kim, J. J., and Masters, B. S. (2000) *J. Biol. Chem. 275*, 21914−21919.
27. Abu-Soud, H. M., Wu, C., Ghosh, D. K., and Stuehr, D. J. (1998) *Biochemistry 37*, 3777−3786.
28. Huang, L., Abu-Soud, H. M., Hille, R., and Stuehr, D. J. (1999) *Biochemistry 38*, 1912−1920.
29. Negrerie, M., Berka, V., Vos, M. H., Liebl, U., Lambry, J.-C., and Martin, J.-L. (1999) *J. Biol. Chem. 274*, 24694−24702.
30. Scheele, J. S., Bruner, E., Kharitonov, V.G., Martasek, P., Roman, L. J., Masters, B. S. S., Sharma, V. S., and Magde, D. (1999) *J. Biol. Chem. 274*, 13105−13110.
31. Wu, C., Zhang, J., Abu-Soud, H. M., Ghosh, D. K., and D. J. Stuehr. (1996) *Biochem. Biophys. Res. Commun. 222*, 439−444.
32. Boggs, S., Huang, L., and Stuehr, D. J. (2000) *Biochemistry 39*, 2332−2339.
33. Abu-Soud H. M., and Hazen S. L. (2000) *J. Biol. Chem. 275*, 37524−32.
34. O'Donnell, V. B., Coles, B., Lewis, M. J., Crews, B. C., Marnett, L. J., and Freeman, B. A. (2000) *J. Biol. Chem. 275*, 38239−44.
35. Glover, R. E., Koshkin, V., Dunford, H. B., and Mason, R. P. (2000) *Nitric Oxide 6*, 439−44.
36. Dweik, R. A., Laskowski, D. Abu-Soud, H. M., Kaneko, F. T., Hutte, R., Stuehr, D. J., and Erzurum, S. C. (1998) *J. Clin. Invest. 101*, 660−666.

BI010066M